

The case for primordial black holes as dark matter

M. R. S. Hawkins^{1*}

¹*Institute for Astronomy (IfA), University of Edinburgh, Royal Observatory, Blackford Hill, Edinburgh EH9 3HJ, UK*

Accepted 1988 December 15. Received 1988 December 14; in original form 1988 October 11

ABSTRACT

The aim of this paper is to present the case that stellar mass primordial black holes make up the dark matter component of the Universe. A near critical density of compact bodies implies that most lines of sight will be gravitationally microlensed, and the paper focuses on looking for the predicted effects on quasar brightness and spectral variations. These signatures of microlensing include the shape of the Fourier power spectrum of the light curves, near achromatic and statistically symmetric variations, and the absence of time dilation in the timescale of variability. For spectral changes it is predicted that as the continuum varies there is little corresponding change in the strength of the broad lines. In all these cases, the observations are found to be consistent with the predictions for microlensing by a population of stellar mass compact bodies. For multiply lensed quasar systems where the images vary independently and microlensing is the generally accepted explanation, the case is made that stellar populations are too small to produce the observed effects, and that the only plausible alternative is a population of compact dark matter bodies of around a stellar mass along the line of sight. The most serious objection to dark matter in the form of compact bodies has come from observations of microlensing of stars in the Magellanic Clouds. In this paper the expected event rate is re-analysed using more recent values for the structure and dynamics of the Galactic halo, and it is shown that there is then no conflict with the observations. Finally, the possible identity of a near critical density of dark matter in the form of stellar mass compact bodies is reviewed, with the conclusion that by far the most plausible candidates are primordial black holes formed during the QCD epoch. The overall conclusion of the paper is that primordial black holes should be seen alongside elementary particles as viable dark matter candidates.

Key words: dark matter – cosmology: observations

1 INTRODUCTION

The nature of dark matter remains one of the biggest unsolved problems in cosmology. Over the last 20 years or so, the identification of dark matter with elementary particles has received widespread support. This idea is primarily motivated by the acceptance that the observed density of dark matter far exceeds the density of baryonic material predicted to be created in the standard Big Bang cosmology, with the implication that the dark matter must be in non-baryonic form. Elementary particles have been seen as the most obvious choice here as, despite the lack of any observational evidence, theoretical predictions from extensions to the standard model of particle physics provide a number of different particles as dark matter candidates. Much effort has been put into detecting such particles directly, but so far there has been no success (Feng 2010). In fact the parameter space to

be searched is very large, and potential dark matter particles have by no means been ruled out, but it is perhaps worthwhile at this stage to review the status of other candidates.

The requirement that dark matter be non-baryonic puts a major constraint on any alternative to elementary particles. In particular, the idea that dark matter is in the form of compact bodies has been treated with some scepticism, as familiar objects such as stellar remnants or brown dwarfs, being baryonic, are ruled out as candidates. However, there are possibilities for compact bodies which are non-baryonic. The most thoroughly investigated of these are primordial black holes. A strong case has been made that in the early Universe density fluctuations could lead to copious production of primordial black holes (Carr & Hawking 1974; Carr 1975). Such black holes are most likely to be formed at epochs when the Universe undergoes phase transitions, with masses dominated by the horizon mass at formation (Jedamzik & Niemeyer 1999). In particular, black holes formed during the QCD phase tran-

* E-mail: mrsh@roe.ac.uk

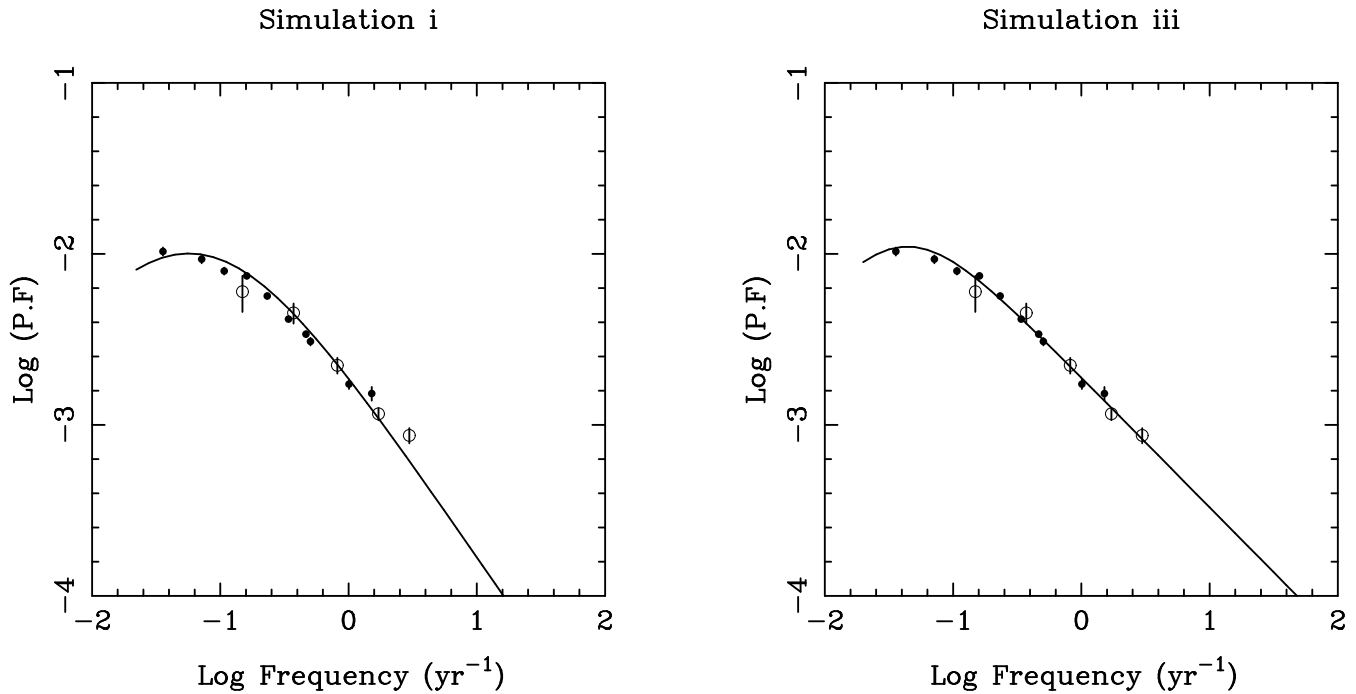


Figure 1. SEDs of light curves in the observer frame for quasars from the Field 287 survey (filled circles) and from the MACHO project (open circles). The solid lines are SEDs for simulated light curves from Minty (2001). In the left hand panel $\Omega_{Lens} = 1.0$ and $\Omega_{\Lambda} = 0.0$. In the right hand panel $\Omega_{Lens} = 0.3$ and $\Omega_{\Lambda} = 0.7$.

sition a few microseconds after the Big Bang should have masses peaking at the QCD horizon mass scale of around $1M_{\odot}$ (Jedamzik 1997). As these objects would be created well before the epoch of baryon synthesis, they would not be subject to the constraints on baryon mass density.

The detection of dark matter in the form of compact bodies has received much attention in the literature. In an early paper, Press & Gunn (1973) pointed out that in a universe where the density of matter is equal to the critical density, every line of sight will be gravitationally lensed. This means that if the dark matter is in the form of compact bodies, they will have the effect of distorting the image of any distant light source. For bodies of around a solar mass the characteristic timescale for changes in brightness is a few years. This domain of gravitational lensing, known as microlensing, opens up the potential for detecting dark matter in this form by observing changes in brightness of distant compact light sources such as quasars. Much work has been done by several groups in simulating the light curves expected from microlensing, with the idea of comparing the results with observed quasar variability (Chang & Refsdal 1979; Paczyński 1986a; Kayser et al. 1986; Schneider & Weiss 1987). There is however a problem with this approach, as any intrinsic quasar variability must be taken into account.

There is one situation where quasar microlensing can be identified unambiguously. There are now many known examples of a massive galaxy producing multiple images by the gravitational lensing of a more distant quasar along the line of sight (Walsh et al. 1979; Huchra et al. 1985). Any intrinsic variation in the quasar will be observed in all images,

with some time difference due to the differing path lengths to the images. However, in all quasar systems which have been adequately observed, it has been found that for the most part individual images vary independently. This is widely recognised as being due to microlensing (Irwin et al. 1989), and supports the idea that all quasars are being microlensed. There is however a caveat, that as these systems are known to have a massive galaxy close to the line of sight, normal stars in this lensing galaxy might be responsible for the microlensing.

Perhaps the best known search for compact bodies is for those in the halo of the Galaxy. By monitoring several million stars in the LMC and SMC, bodies of around a solar mass were detected by the MACHO project (Alcock et al. 2000a). The detection rate of these bodies implies a larger population than can be accounted for by known stellar populations, and so they are clearly good dark matter candidates. However, they have been discounted on the basis that they make up insufficient dark matter for the predictions of models of the Galactic halo consistent with available observations.

The purpose of this paper is to review the arguments that compact bodies in the form of primordial black holes make up the dark matter component of the Universe. We shall firstly look at the evidence for microlensing in quasar light curves, which includes time dilation measures, comparison with microlensing simulations, chromatic changes and statistical symmetry. Much of this work has already been published, but the comparison of the simulations with observations is new, and work on colour changes and symmetry is updated. We derive a further test for microlensing

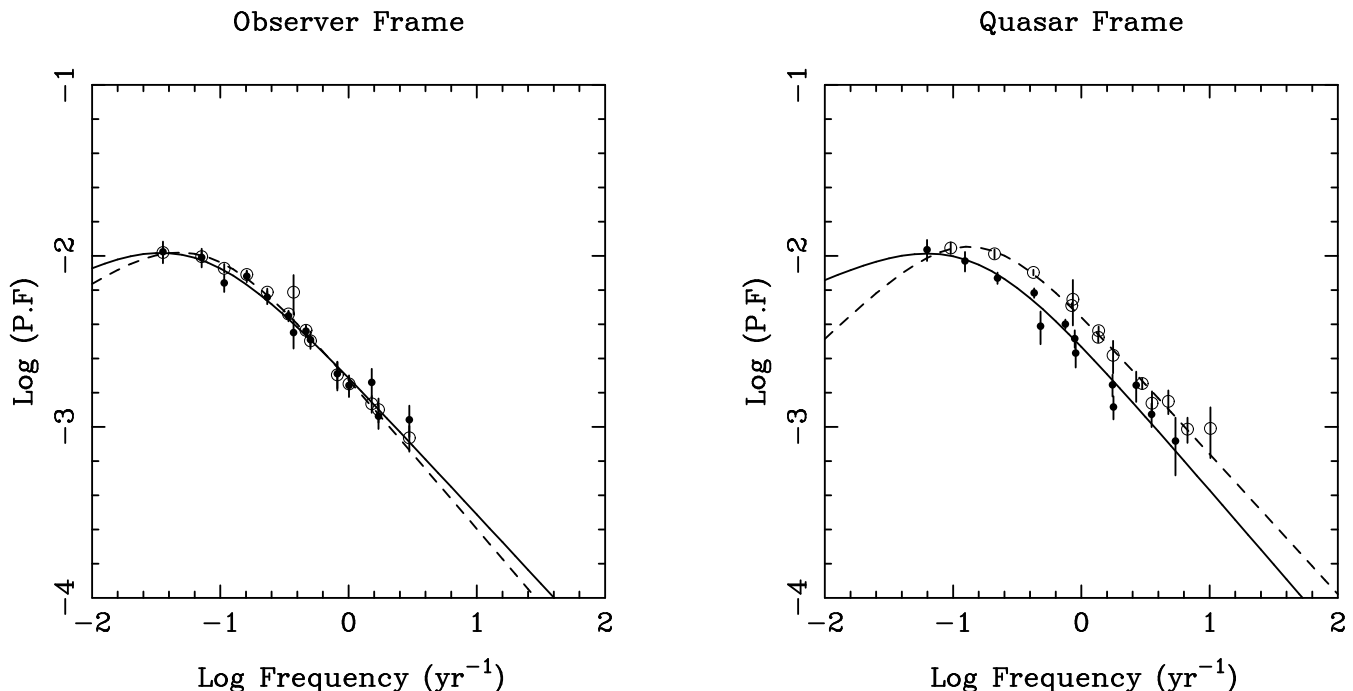


Figure 2. The left hand panel shows the superposition of the SEDs for low redshift (filled circles) and high redshift (open circles) samples of light curves. The solid and dashed lines are best fits of the curve in Eq. 7. The right hand panel shows SEDs of the same light curves in the quasar frame, with a correction for time dilation applied.

by comparing changes in continuum and emission line flux. Although this has been done before, we use new and very much improved data here. We then examine from a new perspective the claim that microlensing in multiply imaged quasar systems is caused by stars in the lensing galaxy. Finally, we use the Galactic halo microlensing observations of the MACHO collaboration together with the most recent measurements of the halo parameters to re-determine the optical depth to microlensing, and hence the limit on dark matter in the form of compact bodies.

2 QUASAR LIGHT CURVES

2.1 Microlensing simulations

If primordial black holes make up the bulk of dark matter, then they should betray their presence by microlensing the light of distant quasars. The structure of the resulting light curves has been the subject of extensive research, in the form of computer simulations and theoretical studies. Fourier power spectrum analysis is perhaps the most useful tool for comparing the observed variability of quasars with the results from numerical simulations, but structure functions and auto-correlation functions have also been used.

We start with some definitions and formulae. The Einstein radius θ_e of a gravitational lens is defined as

$$\theta_e = \left(\frac{4Gm}{c^2 R} \right)^{1/2} \quad (1)$$

which thus varies as the square root of the lens mass m . R is a distance parameter defined by

$$R = \frac{D_{ol} D_{os}}{D_{ls}} \quad (2)$$

with the subscripts indicating angular diameter distances between observer, source and lens; G is the gravitational constant and c is the speed of light. For a solar mass primordial black hole midway to a quasar at a redshift of 1 to 2, θ_e subtends a distance of about 10^{-2} pc or 3×10^{16} cm. For a single isolated lensing event where the source is small compared with the Einstein radius of the lens, the amplification a is given by (Vietri & Ostriker 1983)

$$a = \frac{1 + 2\theta^{-2}}{(1 + 4\theta^{-2})^{1/2}} \quad (3)$$

where θ is the angular distance from the observer's line of sight to the lens in units of the Einstein radius. In the case of microlensing, the change of brightness with time t is thus given by

$$a(t) = \frac{1 + 2\theta(t)^{-2}}{(1 + 4\theta(t)^{-2})^{1/2}}, \quad \theta(t)^2 = \theta_0^2 + v^2(t - t_0)^2 \quad (4)$$

where θ_0 is the minimum distance from the trajectory of the lens to the source in units of Einstein radius, t_0 is the time of closest approach of the lens to the source, and v is the speed of the source in units of Einstein radius per unit time. For multiple lenses there are no simple analytic solutions, and the changes in brightness must be obtained from simulations.

The first simulations of microlensing at large optical

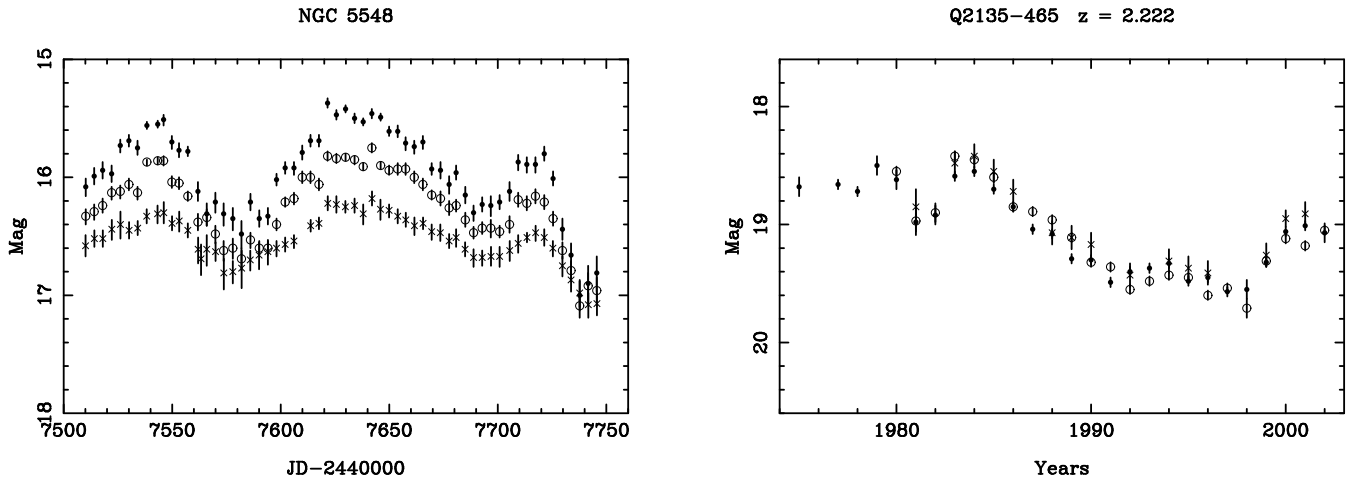


Figure 3. The left hand panel shows continuum ultraviolet light curves for the Seyfert galaxy NGC 5548 from the IUE satellite. The wavelength bands are centred on $\lambda 1350$ (crosses), $\lambda 1840$ (filled circles) and $\lambda 2670$ (open circles). The right hand panel shows optical light curves for a high redshift quasar from the Field 287 survey. The wavelength bands are U (crosses), B_J (filled circles) and R (open circles).

depth were published by Paczyński (1986a). This early work modelled a single plane with randomly placed lenses, and a point source moving across it relative to the observer. Kayser et al. (1986) extended this work using an inverse ray tracing technique, to include the case of extended sources. Improvements in numerical techniques (Schneider & Weiss 1987; Refsdal & Stabell 1991; Lewis et al. 1993) enabled more complicated lens distributions and source parameters to be modelled. For the purposes of comparing the observed quasar light curves with flux variations from microlensing, we shall use the simulations of Minty (2001). We choose these simulations as they are the development of the earlier work cited above, but incorporating a 3-dimensional lens distribution and, importantly for the purposes of this paper, the results are presented in the form of Fourier power spectra of the microlensing variations, which is essential for comparison with observations. The ray tracing procedure is described by Minty et al. (2002), together with an illustration of a simulated microlensing light curve.

In these simulations the lenses are distributed on multiple planes, and move independently with a random velocity drawn from a Gaussian distribution. Rays are traced back from the observer and their position in the source plane recorded, which then enables the magnification pattern to be calculated. The lenses are then moved according to their random velocity and the ray-tracing procedure is repeated, allowing the simulation to evolve over time. The 3-dimensional lens distribution puts great demands on computer power, and so the simulations were carried out on a number of parallel platforms at the Edinburgh Parallel Computing Centre (EPCC).

The magnification patterns in the observer plane allow the variations in brightness due to microlensing to be converted to simulated light curves for sources with specified light profiles. This procedure was used to generate large numbers of light curves for which Fourier power spectra were calculated. This format is well suited to comparing the

Table 1. Simulation parameters.

Sim	Lenses	Planes	M_L	z_s	Ω_M	Ω_L	Ω_Λ
<i>i</i>	100000	5	1	2.0	1.0	1.0	0.0
<i>ii</i>	100000	10	1	2.0	1.0	1.0	0.0
<i>iii</i>	87875	5	1	2.0	0.3	0.3	0.7
<i>iv</i>	23000	5	1	1.0	0.3	0.3	0.7
<i>v</i>	29291	5	1	2.0	0.3	0.1	0.7
<i>vi</i>	2929	5	1	2.0	0.3	0.01	0.7
<i>vii</i>	20000	5	0.1 - 1	2.0	0.3	0.1	0.7

characteristics of microlensing variations with observed light curves, for which Fourier power spectra can also be calculated. The results of the ray tracing procedure depend upon the cosmological model and the proportion of dark matter in the form of compact bodies, and Minty (2001) treats a variety of different cases.

Table 1 is adapted from Minty (2001), and gives parameters for the seven models for which simulations are presented. Column 1 gives the simulation identification, columns 2 and 3 the number of lenses and lens planes. Column 4 gives the range of lens masses in units of M_\odot , and column 5 the redshift of the source. The last three columns list the cosmological parameters for the simulations. Ω_M and Ω_Λ are the conventional contributions to the density parameter from mass and dark energy respectively, and Ω_L is the contribution from lenses alone.

The observations which we shall use for comparison with the simulations are described in detail in Hawkins (2010), and comprise light curves taken from two sources. The first is a large scale yearly monitoring programme of

some 1200 quasars in several passbands covering a total of 28 years (Hawkins 2003; Hawkins 2007). The second is from the MACHO project, where quasars detected as part of the monitoring programme have been identified (Geha et al. 2003). The original observations cover timescales from a few days to several years, and form an important complement to the long term light curves. In order to make a quantitative comparison with the simulations, Fourier power spectra were calculated for the two datasets, as described in Hawkins (2010).

We define the Fourier power spectrum $P(s)$ as:

$$P(s_i) = \frac{t}{N} \left(\sum_{j=1, N} m(t_j) \cos \frac{2\pi i j}{N} \right)^2 + \frac{t}{N} \left(\sum_{j=1, N} m(t_j) \sin \frac{2\pi i j}{N} \right)^2 \quad (5)$$

where i runs over the N equally spaced epochs of observation separated by time t , and $m(t_j)$ is the magnitude at epoch t_j . In the case of a sample of light curves, the integration for each frequency continues over all sample members. We define the SED as a plot of the product of Fourier power and frequency versus frequency.

In Fig. 1 the SEDs of the observed quasar light curves are shown in both panels. The data from the two sources described above are plotted with different symbols, and it will be seen that there is good agreement in the area of overlap. This provides a limit on any systematic differences between the two samples, and a check on the validity of the error bars. The solid lines are the SEDs of simulations of microlensing light curves from Minty (2001). The left hand panel is for an Einstein-de Sitter cosmology with lenses making up the critical density, and the right hand panel for a non-zero cosmological constant, with $\Omega_\Lambda = 0.7$, and all matter in the form of lenses with $\Omega_{Lens} = 0.3$. The position f of the curves on the frequency axis is a measure of timescale of variation t , and in the simulations depends on two free parameters. The first is the Einstein radius which is proportional to the square root of the lens mass M_L , and the second is the mean transverse velocity v_t of the lenses across the line of sight to the source. Hence

$$t \propto \frac{\sqrt{M_L}}{v_t} \propto f^{-1} \quad (6)$$

The characteristic lens mass may thus be measured by adjusting t to fit the simulations to the data. However, it will be seen from Eq. 6 that there is a degeneracy between M_L and v_t . There are a number of components to v_t , which have been measured with varying degrees of accuracy. These include the solar motion relative to the CMB (Kogut et al. 1993), peculiar velocities of galaxy populations (Hawkins et al. 2003), and bulk motions of the intervening material and the source (Hudson et al. 2004; Kashlinsky et al. 2008). Combining these contributions gives $v_t \approx 1300 \text{ km sec}^{-1}$, with a range from 1000 to 1550 km sec^{-1} . Table 2 shows the result of a least squares iterative fit of the simulations to the data, varying M_L for different values of v_t . The resulting lens masses lie in the range 0.08 – 0.23 M_\odot . Both simulations in Fig. 1 have a broadly similar shape to the data, which is independent of the fitting process.

Table 2. Lens masses in units of M_\odot .

v_t (km sec ⁻¹)	1000	1300	1550
Sim <i>i</i>	0.08	0.13	0.19
Sim <i>iii</i>	0.10	0.16	0.23

Although the good agreement between the SEDs of the observed light curves and the microlensing simulations does not show that quasars are being microlensed, it does demonstrate that if dark matter is in the form of stellar mass compact bodies, then the variations expected from microlensing simulations are consistent with observations of quasar light curves.

2.2 Time dilation

The idea that primordial black holes are microlensing the light of quasars can be tested quite simply by looking for the effects of time dilation in quasar light curves. If the observed variations are intrinsic to the quasar, then whatever their origin, they should show a stretching of timescale with redshift by a factor $(1+z)$. If on the other hand the observed variations are dominated by the effects of microlensing, then no such change in timescale will be seen. This is because the variations no longer originate in the quasar rest frame, but at the redshift of the lenses. Due to the curvature of space at high redshift, it turns out that the probability distribution for the position of lenses is strongly peaked close to a redshift $z = 0.5$, regardless of the redshift of the source (Turner et al. 1984). This result is insensitive to the assumed cosmology, and means that the effects of time dilation on quasar light curves from microlensing will be small. Consequently there will be little difference in the characteristic timescales of low and high redshift samples.

The task of looking for time dilation in quasar light curves was addressed in a recent paper (Hawkins 2010) using the data discussed earlier in this Section. The light curves were divided into high and low redshift samples, with the additional constraint of a restricted range in absolute magnitude, to prevent any confusion with possible luminosity effects. SEDs for the light curves from the two redshift samples were calculated as described above, and are plotted in Fig. 2. The idea was to look for a shift to longer timescales for the high redshift sample relative to the lower redshift one. To aid comparison, the two SEDs were fitted with a double exponential function of the form:

$$P(f) = \frac{C}{\left(\frac{f}{f_c}\right)^a + \left(\frac{f}{f_c}\right)^{-b}} \quad (7)$$

The left hand panel shows the high and low redshift SEDs superimposed, and it is clear that no shift is observable. The right hand panel shows the the same data, but with a correction for time dilation applied. This has the effect of preferentially moving the high redshift sample to shorter

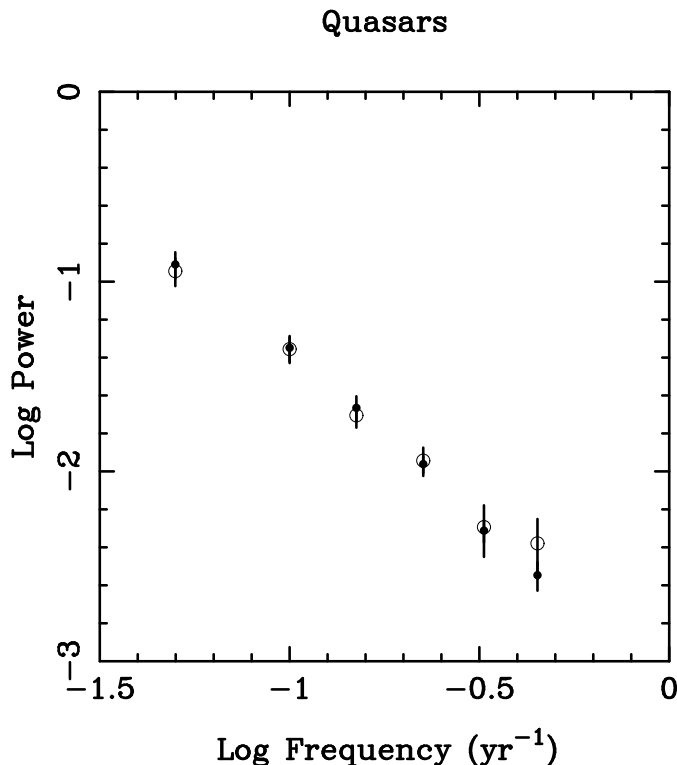


Figure 4. Fourier power spectra for a sample of 75 quasar light curves in B_J (filled circles) and R (open circles). The sample limits are $z > 1.5$ and $M_B < -26$.

timescales. This gives an idea of the expected shift between the two curves if time dilation were present.

If primordial black holes are the main constituent of dark matter, then they should cause large variations in quasar light, and these variations will not show the effects of time dilation. The data in Fig. 2 supports this prediction, and also implies that quasar variation from microlensing dominates any intrinsic process. Although this does not necessarily establish that quasars are being microlensed, alternative explanations for the observations are not easy to find.

2.3 Colour changes

The study of colour changes in AGN has received extensive attention from campaigns to measure the change in emission line strength relative to continuum luminosity in Seyfert I galaxies (Peterson et al. 2002). These observations are designed to measure time delays between nuclear variations and emission line response, but they also show without any doubt that the nucleus changes colour in the sense that, as it brightens, it becomes bluer. The left hand panel of Fig. 3 shows light curves of the nucleus of the Seyfert I galaxy NGC 5548 in three ultra-violet bands from the IUE satellite (Clavel et al. 1991). The data have been converted to magnitudes on an arbitrary scale, and show quite clearly the change of colour with brightness. The distance to NGC 5548 is much too small for any variations in brightness to be caused by microlensing, but we now investigate the situation at higher redshift where gravitational lensing is a possibility. A well known property of gravitational lensing is that

for a uniformly illuminated or point source, the effects of the lensing will be achromatic as photon trajectories are independent of colour. If quasars are being microlensed by primordial black holes, one might therefore expect that the variations would be achromatic. This will be the case provided that quasars are point sources, in the sense that they only emit light from within an angle that is small compared with the Einstein radius of the lens. However, dilution of the nuclear light by light from the host galaxy, or an extended emission region with a colour gradient around the nucleus itself, will cause the quasar to change colour as it brightens or fades. The procedure for correcting for the effect of the host galaxy on a quasar light curve has been examined in some detail by Hawkins (2003). Here we shall confine ourselves to the straightforward case where the nucleus is sufficiently luminous for the observed variations not to be significantly affected by the underlying galaxy.

The right hand panel of Fig. 3 shows light curves for a luminous quasar in the U , B_J and R bands. The wavelengths of these bands in the quasar rest frame are close to the wavelengths of the ultra-violet bands in the left hand panel, and provide an interesting comparison between the modes of variation of the two objects. It is clear that in contrast to the Seyfert galaxy, the variations of the quasar are essentially achromatic.

The contrast between the two objects in Fig. 3 may be put on a statistical footing by comparing the spectrum of variations of a large sample of red and blue passband quasar light curves. Fig. 4 shows Fourier power spectra for 75 such light curves of luminous quasars ($M_B < -26$), and it will be seen that the two spectra have the same power at all frequencies. This implies that the variations of the sample as a whole are achromatic.

2.4 Symmetry

It is clear from Eq. 4 that in the restricted case of a single point source, the brightness variation will be symmetrical in time. However, in a situation where multiple lenses are involved, the variation is much more complicated. The amplification patterns combine in a non-linear way to produce variations with no obvious symmetrical structure. The resulting light curve will however be statistically symmetric in the sense that there will be no preferred direction of time. In other words it will not be possible to distinguish between running time forwards or backwards by examining the variations alone.

The measurement of statistical symmetry in quasar light curves has been addressed in an interesting paper by Kawaguchi et al. (1998). They present an accretion model of quasar variability which is predicted to lead to asymmetrical variations in the sense that the brightness of the nucleus will rise more slowly than it falls. To measure this asymmetry they define a modification of the structure function S which may be defined by

$$S(t) = \sqrt{\frac{1}{N(t)} \sum_{i < j} [m(t_j) - m(t_i)]^2} \quad (8)$$

where $m(t_i)$ is the magnitude measure at epoch t_i , and the sum runs over the $N(t)$ epochs for which $t_j - t_i = t$. In addition to the standard structure function defined above, we

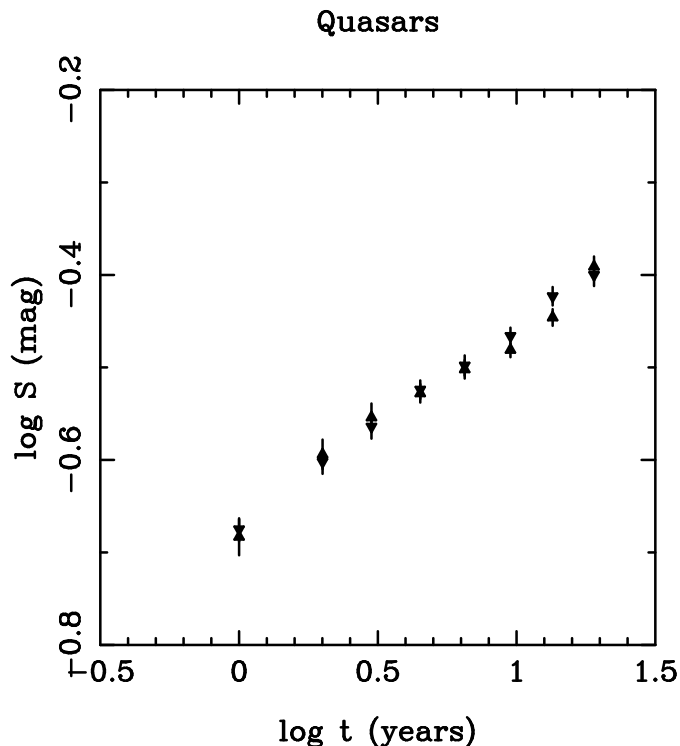


Figure 5. Time asymmetric structure functions for a sample of 366 quasar light curves. Functions for increasing and decreasing brightness are shown by upward and downward pointing triangles respectively. The sample limits are $z > 1.5$ and $M_B < -23$.

shall for the purpose of measuring asymmetries also make use of two modified structure functions S_+ and S_- . These are defined as for S except that for S_+ the integration only includes pairs of magnitudes for which the flux becomes brighter, and S_- for which it becomes fainter.

Kawaguchi et al. (1998) calculate the functions S_+ and S_- for simulated light curves from their accretion model and show that there is more power in S_- implying a gradual rise and rapid decay in flux. This is a common feature of accretion models, and a plausible mechanism for intrinsic variation in quasars. If dark matter is in the form of primordial black holes, then the microlensing effect should result in time symmetric variation as discussed above, with no difference between S_+ and S_- .

Fig. 5 shows S_+ and S_- calculated for a sample of quasar light curves from Field 287. The two curves are not distinguishable within the errors of observation, implying that the variations are time symmetric. Although this certainly does not rule out the possibility that the quasar variations are intrinsic, it is as expected for microlensing by primordial black holes.

3 SPECTRAL CHANGES IN QUASARS

An important diagnostic for the origin of AGN variability is the analysis of correlations between emission line and continuum variations. Reverberation mapping studies of Seyfert I galaxies, notably NGC 5548 (Peterson et al. 2002), have conclusively shown that changes in continuum flux are followed after a few days by a corresponding change

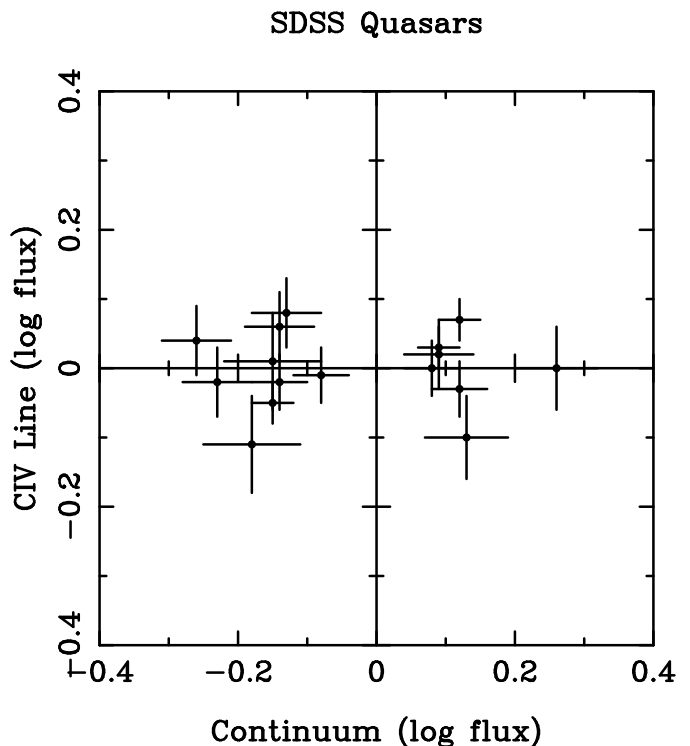


Figure 6. Change in CIV line flux versus change in continuum flux adapted from Wilhite et al. (2006)

in broad emission line flux. The way this is generally understood is that the broad emission line region surrounding the accretion disc and supermassive black hole is responding to changes in the central photon flux with corresponding changes in line flux. The time delay is seen as a measure of the photon travel time from the central engine to the broad line region and hence a measure of its size.

For quasar variations caused by microlensing, the changes in spectrum are predicted to follow a different pattern as a result of the different sizes of the continuum and broad line emitting regions. The effect of source size on gravitational lens amplification has been the subject of a number of investigations. Refsdal & Stabell (1991) derived a simple analytical formula for estimating the typical microlensing amplification δm for sources larger than the Einstein radius of the lenses, compared to the amplification of point sources:

$$\delta m \approx \frac{2.17\sqrt{|\sigma|\theta_e M}}{\theta} \quad (9)$$

Here, σ is the normalised surface density in stars, θ_e the Einstein radius for the effective mass M of the microlensing stars, and θ is the angular radius of the source. These parameters are described in more detail by Refsdal & Stabell (1991). The important point to notice is a decrease in amplification magnitude δm for source size θ scaling as $(\theta/\theta_e)^{-1}$, which is consistent with results from microlensing simulations (Kayser et al. 1986; Schneider & Weiss 1987; Lewis et al. 1993). The size of the luminous part of AGN accretion discs r_s has been measured from microlensing in multiply lensed quasar systems by several groups (Pelt et al. 1998; Kochanek 2004; Morgan et al. 2010). The results are in good agreement, giv-

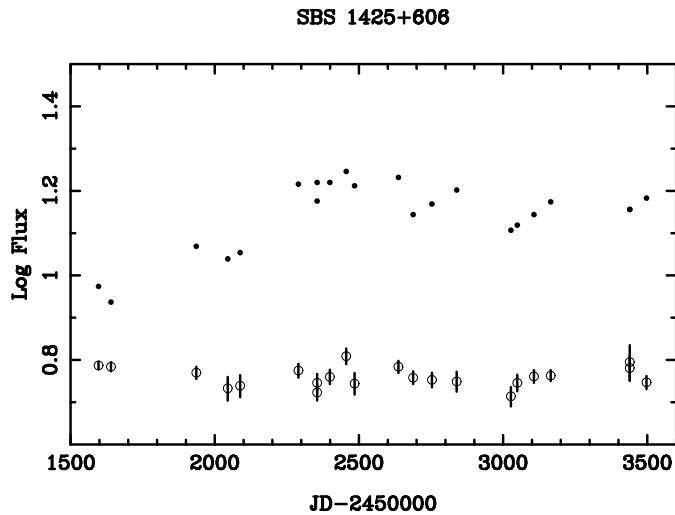


Figure 7. Light curves for the quasar SBS 1425+606 adapted from Kaspi et al. (2007). Continuum flux is shown as filled circles, and the C IV $\lambda 1550$ line flux as open circles.

ing a value $r_s \sim 3 \times 10^{15}$ cm. The size of the Einstein radius for a solar mass star from Eq. 1 is some 10 times larger than this, which is sufficient for the quasar disc to be microlensed as a point source (Lewis et al. 1993).

The extent to which the broad emission lines in quasar spectra will be microlensed depends upon the size of the broad line region (BLR). There have been extensive efforts to measure the distance of the BLR from the central source of continuum flux using reverberation mapping techniques, with the primary motive of measuring the mass of the central black hole. The results show (Kaspi et al. 2005) that for quasars, the size of the BLR is typically in excess of 100 light days, or 3×10^{18} cm. This is 100 times larger than the Einstein radius for a solar mass body, resulting in negligible microlensing amplification of the BLR (Refsdal & Stabell 1991).

If microlensing by stellar mass primordial black holes is the cause of variations in quasar brightness then the results of this Section imply that changes in continuum flux will not be accompanied by changes in emission line flux. This contrasts with the situation where there are intrinsic changes in continuum flux, in which case the broad emission line flux will follow changes in the continuum. To test for this, we shall make use of spectrophotometric monitoring programmes which have measured continuum and broad line flux in quasar spectra at different epochs.

Fig. 6 shows the change in C IV $\lambda 1550$ flux as a function of change in continuum flux from a sample of quasars from the Sloan Digital Sky Survey (SDSS) (Wilhite et al. 2006). All quasars from the sample are included which have $S/N > 8$ for both epochs, and a time lag $\Delta t > 100$ days. It will be seen that although the continuum varies by over half a magnitude in both directions, there is no corresponding change in C IV flux.

A more detailed picture of the way the spectrum changes is given in Fig. 7. This shows continuum and C IV $\lambda 1550$ light curves for the quasar SBS 1425+606, adapted from Kaspi et al. (2007). We first note that within each year,

on a timescale of a few weeks, there is some evidence of a weak correlation between continuum and line flux changes. This presumably corresponds to a response of the BLR to changes in continuum strength, as seen in Seyfert galaxies such as NGC 5548 (Peterson et al. 2002). However, the continuum light curve is clearly dominated by a rise of 0.6 magnitudes over a period of about 2 years, followed by a gentle decline. This has no counterpart in the C IV flux, which remains constant to within ± 0.1 magnitudes.

4 THE GALACTIC HALO

One of the most powerful tests for dark matter in the form of primordial black holes, or any other compact bodies, is to search for them in the halo of the Milky Way. An ingenious procedure for doing this was proposed by Paczyński (1986b), which led to the setting up of the MACHO project. The idea behind this well known project was to photometrically monitor several million stars in the Magellanic clouds, to search for the rare event when one of them was microlensed by a compact halo object (MACHO). This project was challenged by a number of formidable difficulties, including the creation and running of a suitable photometric pipeline, a robust algorithm for detecting microlensing events, a reliable estimator for detection efficiency and an accurate model of the Milky Way halo. Despite these difficulties, the project yielded excellent results and three microlensing events were detected in the first year (Alcock et al. 1996). This increased to 17 events when the project was completed some 6 years later.

Despite the success of the detection of microlensing events, the results appeared ambiguous. The team estimated that the detections only accounted for 20% of the mass of a typical halo model, and that a halo consisting entirely of compact bodies could be ruled out at 95% confidence level for all but their most extreme halo model. On the other hand, the population of compact bodies implied by the microlensing detections was substantially larger than all known stellar populations (Alcock et al. 2000a). These conclusions have been sufficient to create a consensus that dark matter is not made up of compact objects, and to look to elementary particles to provide alternative candidates. However, the identity of the objects that were detected still remains unclear.

Since the publication of the MACHO survey results (Alcock et al. 2000a) there has been much discussion and disagreement about the reliability of event classification, the location of the lenses and the estimation of detection efficiency (Bennett et al. 2005 and references therein). There are several phenomena which can mimic microlensing events, including certain types of variable star and supernovae, and different classification procedures often do not agree. The location of the lenses presents an additional source of uncertainty. As well as lenses in the Galactic halo which were the target of the MACHO project, microlensing events can in principle also be caused by stars in the LMC itself, or in the Galactic disc. There seems little doubt that some lensing events have been mis-classified, but there is still disagreement about how many and which ones (Bennett et al. 2005). A crucial part of the process for determining the MACHO content of the halo is the estimation of the detection effi-

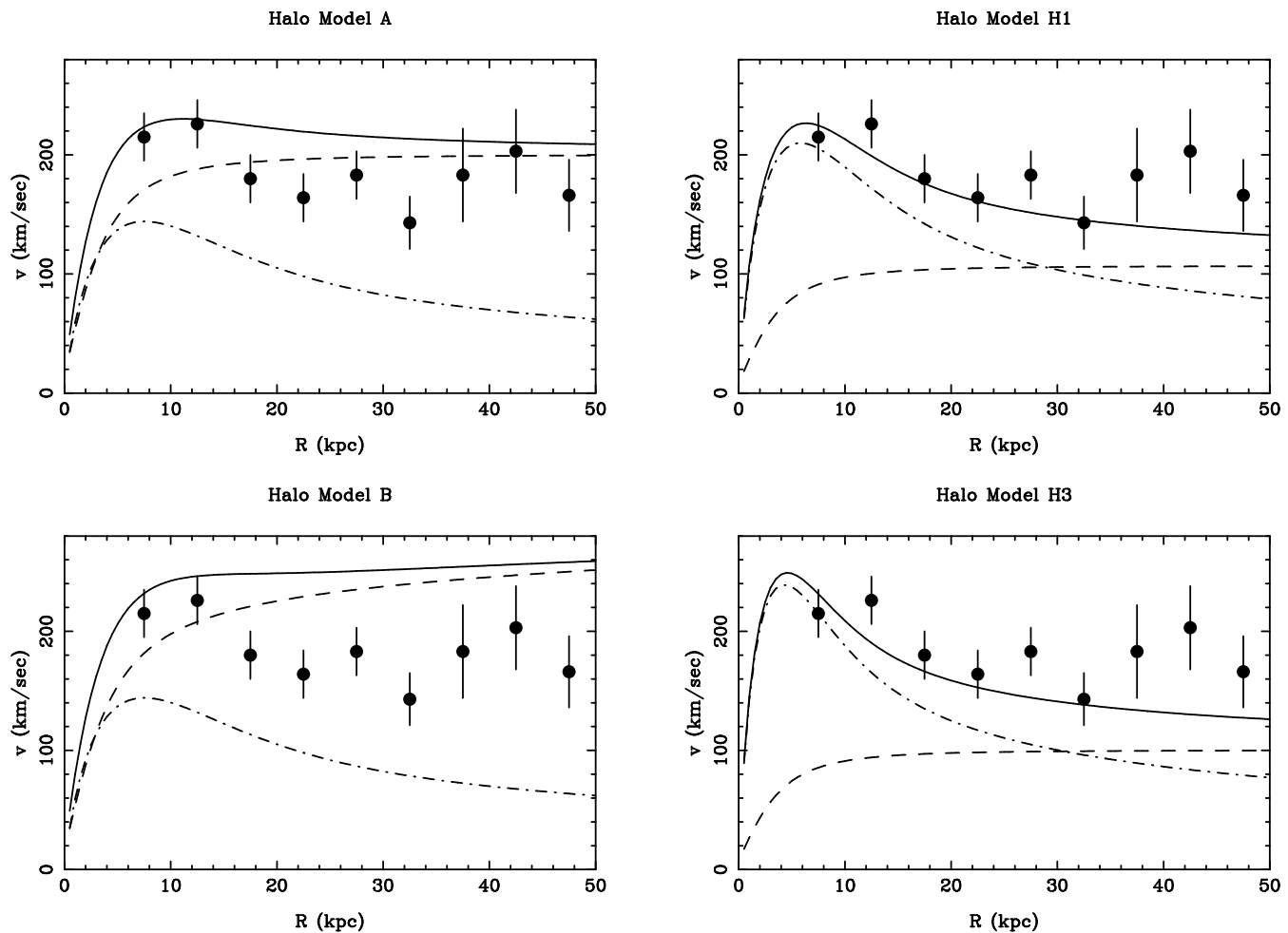


Figure 8. Rotation curves for models of the Galactic disc and halo. The disc and halo components of the rotation curve are shown as dash/dot and dashed lines respectively, and the combined rotation curve by a solid line. The observed rotation curve derived from SDSS observations of BHB stars (Xue et al. 2008) is shown as filled circles.

ciency (Alcock et al. 2000b). Not all lensing events that take place during the period of the survey will be detected, and to convert the detections which are made to the actual halo population of MACHOs requires a complex computer simulation. There are many parameters involved in the detection probability of an event, including maximum magnification, Einstein radius crossing time, time of peak magnification, observing programme, weather conditions and overlaps by neighbouring stars. In addition the computer model requires a knowledge of the stellar luminosity function across the Magellanic clouds, the distribution of blended images and how this affects photometric accuracy. The MACHO collaboration have done a careful job in modelling these effects, but there are many uncertainties which could result in either an increase or decrease in the size of the observed MACHO population of the halo, and no way of making an external check on the accuracy of the detection efficiency. With these caveats in mind we shall adopt the published results of the MACHO collaboration (Alcock et al. 2000a) in what follows here.

An important measure of the mass of a population of compact bodies in a galaxy halo is the optical depth to microlensing τ , defined as (Alcock et al. 1996)

$$\tau = \frac{4\pi G}{c^2} \int_0^L \rho(l) \frac{l(L-l)}{L} dl \quad (10)$$

where L is the distance from observer to source. This is effectively the probability that a source is being microlensed by a compact body along the line of sight. The calculation of τ require a knowledge of the distribution of microlensing mass between the source and observer, which in the case of the MACHO project means a knowledge of the mass profile of the Galactic halo. The MACHO collaboration have made it clear from the start that their conclusions rely heavily on the chosen halo model (Alcock et al. 1995) since, although they can measure quite accurately the MACHO mass within the distance to the LMC, the total halo mass fraction in MACHOs is model dependent. For their analysis they use a standard model of the form

Table 3. Galactic models for LMC microlensing.

Model	S	B	F	H1	H2	H3
β	-	-0.2	0	0	0	0
q	-	1	1	1	1	1
R_c (kpc)	5	5	25	5	5	5
R_0 (kpc)	8.5	8.5	7.9	8.5	8.5	8.0
Σ_0 ($M_\odot \text{pc}^{-2}$)	50	50	80	67	50	50
R_d (kpc)	3.5	3.5	3.0	2.7	2.3	2.0
Θ_0 (km s^{-1})	192	233	218	220	220	226
τ_{LMC} (10^{-7})	4.7	8.1	1.9	1.58	1.64	1.45

$$\rho(r) = \rho_0 \frac{R_0^2 + R_c^2}{r^2 + R_c^2} \quad (11)$$

and power law models from Evans (1994), where the density ρ is given by

$$\rho(R, z) = \frac{v_a^2 R_c^\beta}{4\pi G q^2} \times \frac{R_c^2(1 + 2q^2) + R^2(1 - \beta q^2) + z^2[2 - q^{-2}(1 + \beta)]}{(R_c^2 + R^2 + z^2 q^{-2})^{(\beta+4)/2}} \quad (12)$$

where R is the distance from the galactic centre and z is the height above the plane of the disc. q is an ellipticity parameter, β determines whether the rotation curve is rising or falling, v_a is a normalisation velocity and R_c is the halo core radius. Full details of the model are given by Evans (1994). The MACHO collaboration galaxy model also incorporates an exponential thin disc with surface density Σ given by

$$\Sigma(R) = \Sigma_d \exp -R/R_d \quad (13)$$

where Σ_d is a normalization parameter and R_d is the disc scale length.

The MACHO collaboration defined a number of model galaxies with values for β , q , R_c and R_d . They also set values for the sun's galactocentric distance R_0 , the sun's circular speed Θ_0 and the local column density Σ_0 . This then sets values for the normalization parameters v_a and Σ_d . These parameter values were intended to span the range of currently accepted measurements. The collaboration then calculated the optical depth τ for stars in the LMC for each halo model, for comparison with the optical depth calculated from their monitoring programme. In the first year of observations, the three detections yielded an optical depth $\tau = 0.88 \times 10^{-7}$ (Alcock et al. 1996). This changed to $\tau = 2.9 \times 10^{-7}$ after the second year (Alcock et al. 1997), and converged to $\tau = 1.2 \times 10^{-7}$ at the completion of the observations after 5.7 years (Alcock et al. 2000a). In this final paper the MACHO collaboration chose to restrict their halo models to three, shown in Table 3 as models S, B and F, spanning the full range of predicted optical depth to lensing. On this basis they concluded that even their most extreme model was excluded, and that a 100% MACHO halo was ruled out at a 95% confidence level.

The predicted optical depth to microlensing τ is sensitive to most of the parameters listed in Table 3, and

the values used by the MACHO collaboration reflect the best measurements or estimates available at the time (Alcock et al. 1996). Since then, there has been much observational work on the values of these parameters, and there now seems to be a case for reviewing the MACHO limits on the basis of the new data. With this end in view we shall rework the analysis of the MACHO collaboration for a new set of models with parameters in line with recent observational developments.

We first consider the halo core radius R_c . This parameter has conventionally been taken to have a value $R_c \sim 5$ kpc, as suggested by Griest (1991), and supported by the work of Donato et al. (2004). The values of 20–25 kpc used by Alcock et al. (1996) for all their big disc models cannot any longer be justified by current observations. In fact, providing R_c is less than R_0 it makes little difference to the value of τ , and so we shall keep $R_c = 5$ kpc for our new halo models. An important parameter in the Galactic model is the disc scale length R_d , for which Alcock et al. (1996) use values of 3–3.5 kpc. More recent work on the direct measurement of R_d gives scale lengths in the range 2.0–2.7 kpc (Ojha 2000; Siegal et al. 2002; Jurić et al. 2008), and we shall use values in this range for our models. Estimates of the distance to the Galactic centre R_0 and the sun's circular speed Θ_0 have not changed greatly in recent years, and we adopt the same range of values as Alcock et al. (1996). Recent work on the local column density Σ_0 (Korchagin et al. 2003) supports the value of $48 M_\odot \text{pc}^{-2}$ from Kuijken & Gilmore (1991), and there seems to be little observational support for the large values used by the MACHO collaboration for their big disc models. We do however include the value of $67 M_\odot \text{pc}^{-2}$ from Siebert et al. (2003) in one of our models.

The calculation of the optical depth τ was carried out using the procedure described by Alcock et al. (1996). After reproducing their results, τ was calculated for a wide variety of disc/halo models. It was found that with the new range of parameter values discussed above, there was no difficulty in defining a halo such that the optical depth to microlensing lay within 1σ of $\tau = 1.2^{+0.4}_{-0.3} \times 10^{-7}$, the value found by Alcock et al. (2000a) after 5.7 years of observation. The parameters for three examples of halos which are not excluded by the MACHO collaboration confidence limits are given in Table 3 as H1, H2 and H3.

We now consider the sensitivity of the optical depth τ to changes in the halo parameters. This was estimated by recalculating τ for the halo models in Table 3, but changing each parameter in turn by 1% and keeping the remainder constant. The resulting change in τ is thus a measure of the sensitivity to that parameter, and is shown in Table 4 as a percentage, + or – indicating an increase or decrease in τ with increase in the parameter. τ turns out to be most sensitive to R_0 , the distance to the Galactic centre. However, as discussed by Olling & Merrifield (2000), R_0 and Θ_0 are not independent, the ratio Θ_0/R_0 being tightly constrained by measures of the proper motion of SgrA* (Reid et al. 1999). This results in little change in τ for large changes in R_0 . There is little room for the local column density Σ_0 to be much less than $50 M_\odot \text{pc}^{-2}$, as visible matter is estimated to make up some $53 M_\odot \text{pc}^{-2}$ (Holmberg & Flynn 2004). Larger values result in a decrease in the value of τ , implying a lower expected rate for microlensing. The scale length of

Table 4. Sensitivity of optical depth τ to halo parameters.

q	R_c	R_0	Σ_0	R_d	Θ_0
-0.6	+0.6	-14.6	-4.6	+8.8	+11.0

the Galactic disc R_d is one of the most uncertain parameters, and τ is moderately sensitive to it. This is because for given values of R_0 and Θ_0 , the gravitational effect of a more massive disc must be compensated for by a less massive halo, leading to a smaller value for τ . On the whole, measurements of R_d have tended to become smaller, but Table 3 reflects the range of currently supported values. For the remaining parameters, τ is relatively insensitive to R_c and q , and changing β over the range covered by Alcock et al. (1996) only results in a small change in τ .

Fig. 8 illustrates a selection of the rotation curves from the halo models in Table 3. In each case the solid line shows the rotation curve for the model, made up of contributions from the halo and disc. Also shown is the rotation curve derived from SDSS observations of some 2400 blue horizontal branch stars by Xue et al. (2008). Alcock et al. (1995) point out that each set of parameters should give a model consistent with the measured Milky Way rotation curve. The two left hand panels show rotation curves for massive halo models, which clearly do not provide an adequate fit to the observed rotation curve. In this context they consider their Model F to have an extremely low mass halo, ‘somewhat inconsistent with the known Galactic rotation curve’ (Alcock et al. 2000a). In fact, Model F has rotation speed at 50 kpc of 160 km s^{-1} , which is close to the value from the more recent rotation curve of Xue et al. (2008). The right hand panels of Fig. 8 show two halo models from Table 3 with optical depth to microlensing τ not excluded by the MACHO collaboration limits (Alcock et al. 2000a), and values of χ^2 giving an adequate goodness-of-fit to the observations. The implication of this is that using more recent measurements of the structural parameters of the Galactic disc and halo, and the rotation curve of the Milky Way, the MACHO collaboration results do not exclude a dark matter halo consisting entirely of compact bodies.

5 MULTIPLY LENSED QUASARS

One situation in which quasar microlensing can be unambiguously identified is in multiply lensed quasar systems. These systems usually arise when a massive galaxy lies close to the line of sight to a quasar. The galaxy acts as a gravitational lens, and splits the quasar light, typically into two or four images. In these systems it is well established that the individual quasar images vary partly synchronously with a short time gap, and partly independently. The variations which are seen in both images are taken to be associated with intrinsic variations of the quasar nucleus, and the time difference is a measure of the difference in path length to the

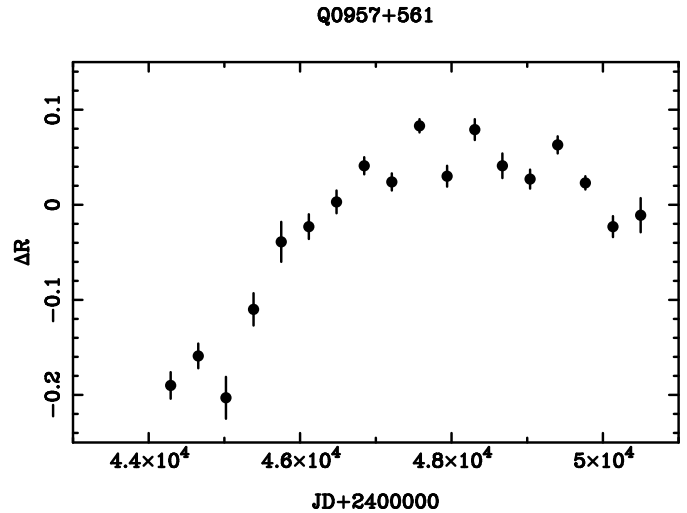


Figure 9. Difference light curve from 1979 to 1997 for the two images of the gravitational lens system Q0957+561. The filled circles are yearly weighted means of observations described by Schild & Thomson (1995) and listed at <https://www.cfa.harvard.edu/~rschild/fulldata2.txt>

two images. However, in all systems which have been studied in sufficient detail the images also vary independently, and this is generally accepted as being due to microlensing by compact bodies along the light paths, where each image would be affected differently.

It is tempting to interpret this microlensing as persuasive evidence that quasars are being microlensed by a cosmological distribution of compact dark matter bodies, but there is an important caveat. By their very nature, in these quasar systems there will always be a massive galaxy close to the line of sight, and typically the quasar light paths will pass through this galaxy. It has generally been assumed that the stellar population in the lensing galaxy is sufficient to provide the population of lensing bodies, but because of the sparse distribution of stars in galactic halos this assumption may not always be reliable.

The gravitational lens system Q0957+561, comprising two quasar images and a massive elliptical lensing galaxy, is well suited to investigating the feasibility of microlensing by stars in the lensing galaxy. Since its discovery in 1979 (Walsh et al. 1979), the brightness of the two images has been intensively monitored by several groups. Schild & Thomson (1995) collate many of the earlier observations, which are tabulated at <https://www.cfa.harvard.edu/~rschild/fulldata2.txt>. Fig. 9 shows the difference between the R magnitudes of the two images as a function of time, covering the period from 1979 to 1998. Yearly weighted means were taken for the two images A and B , using the observational errors given with the data. The difference in magnitude m was then plotted in the sense $\Delta R = m_A - m_B$, with error bars showing the dispersion of the measures within each yearly epoch.

The variation of around 0.3 mag seen in Fig. 9 is generally accepted as being due to microlensing, as no other plausible mechanisms have been suggested. It is also a lower limit on the total microlensing amplitude, since when both images are brightening or fading, it underestimates the vari-

ation in each image separately. We now address the question of whether this microlensing is likely to be due to stars in the lensing galaxy.

The lensing galaxy for the Q0957+561 system is a giant elliptical lying close to the line joining the two images. For Hubble constant $H_0 = 70 \text{ km sec}^{-1} \text{ Mpc}^{-1}$, the distances from the centre of the galaxy to images A and B are 41.9 kpc and 8.9 kpc respectively. The photometry and morphology of this galaxy have been studied in some detail by Bernstein et al. (1997) using WFPC2 observations from the HST. They fit elliptical profiles to the galaxy image which gives surface brightness values of 25.2 and 22.6 $V \text{ mag arcsec}^{-2}$ at the positions of the A and B images respectively. We convert these surface brightnesses to mass surface densities Σ using a mass-to-light ratio for old stellar populations derived from globular clusters (McLaughlin & van der Marel 2005). Adopting $M_\odot/L_\odot = 2$ as a representative value gives $\Sigma_A = 5.2 M_\odot/L_\odot \text{ pc}^{-2}$ and $\Sigma_B = 56.9 M_\odot/L_\odot \text{ pc}^{-2}$.

To calculate the optical depth to lensing τ_A and τ_B for images A and B we use a modified version of Eq. 10:

$$\tau = \frac{4\pi G}{c^2} \frac{\Sigma D_g (D_q - D_g)}{D_q} \quad (14)$$

where D_g and D_q are the distances to the lensing galaxy and quasar respectively. Using the values for Σ_A and Σ_B derived above we obtain $\tau_A = 4.0 \times 10^{-3}$ and $\tau_B = 4.4 \times 10^{-2}$. These low optical depths to lensing imply that a strong microlensing feature of the type illustrated in Fig. 9 is very unlikely to be produced by stars in the lensing galaxy. This leaves two other possibilities. If the dark matter in the lensing galaxy were in the form of compact bodies, then the probability of microlensing would be much larger. Alternatively, a cosmological distribution of dark matter in the form of compact bodies could be responsible for the observed microlensing. Either way, this result implies dark matter in the form of stellar mass compact bodies.

6 CANDIDATES FOR COMPACT DARK MATTER

Hitherto in this paper we have summarised the evidence supporting the idea that dark matter is predominantly in the form of compact bodies, the most plausible candidates being primordial black holes. In this section we shall consider the various possibilities in more detail.

6.1 Baryonic bodies

Perhaps the most plausible candidates for compact dark matter bodies are low mass stars and stellar remnants. For stars with mass $M > 0.1 M_\odot$ the observed background radiation density puts tight constraints on Ω_* , the stellar contribution to dark matter, and on this basis Carr (1994) finds $\Omega_* < 0.1$. For stars with $M < 0.1 M_\odot$ Gilmore (1999) uses arguments for the universality of the IMF and direct mid-infrared observations to constrain the contribution of Ω_* in galactic halos to negligible proportions. Notwithstanding observations such as these, there would always remain the possibility that baryonic matter could remain hidden in some unexpected form were it not for the constraints of cosmological nucleosynthesis, which we now consider.

The standard theory of primordial nucleosynthesis makes predictions for the abundance of the light elements D, ^3He , ^4He and ^7Li . These abundances depend, with varying sensitivity, on the baryon to photon ratio η . Comparison of the predictions with astronomical observations of the abundances only shows consistent agreement over a narrow range of η . This consistency has the dual effect of giving strong support to the standard theory of primordial nucleosynthesis, and providing a robust measure of η . The photon density may be readily obtained from measures of the Cosmic Microwave Background, giving a value for the baryon density Ω_b in the range $0.011h^{-2} < \Omega_b < 0.15h^{-2}$ (Smith et al. 1993). For $H_0 = 70 \text{ km sec}^{-1} \text{ Mpc}^{-1}$ this gives $\Omega_b < 0.03$. This limit effectively rules out any candidates for dark matter in the form of compact bodies which are made up of baryons, and certainly excludes familiar bodies such as stars and planets and any remnants of their evolution.

6.2 Primordial black holes

The only non-baryonic compact bodies which have so far been seriously proposed as dark matter candidates are primordial black holes (Carr 1994). Hawking (1971) showed that density fluctuations in the early Universe could lead to gravitational collapse, and Carr & Hawking (1974) argued that this collapse could lead to the formation of black holes of around the horizon mass M_h at time t , where

$$M_h(t) \approx \frac{c^3 t}{G} \quad (15)$$

Carr (1975) examined the expected primordial black hole mass spectrum, and concluded that the density fluctuations invoked to seed the formation of galaxies are of a type to favour primordial black hole production over a large mass range. As density fluctuations larger than the horizon size enter into the particle horizon they can be close to their Schwarzschild radius, and depending on the balance between pressure and gravity may collapse to become black holes. For a hard equation of state where pressure p and energy density ρ are equated by $p = \rho/3$, regions with overdensity $\delta\rho/\rho \gtrsim 1/3$ should collapse into black holes of the order of the horizon mass M_h from Eq. 15. Fluctuations smaller than this will tend to disperse due to pressure forces. For a soft equation of state where $p \approx 0$, black holes should form much more readily from small relic adiabatic perturbations. The problem with this approach as it stands is that a scale invariant power spectrum normalised to the CMB fluctuations produces a negligible density of primordial black holes.

During phase transitions in the early Universe, and in particular during the quark-hadron transition of the QCD epoch at a cosmic epoch of $\sim 10^{-5} \text{ sec}$, the equation of state is expected to soften. Jedamzik (1997) concluded that the primordial black hole mass function should show a pronounced peak at the QCD mass scale $M_{QCD} \approx 1 M_\odot$. This result was confirmed by general relativistic hydrodynamic numerical simulations which showed that the fluctuation density threshold $\delta\rho/\rho$ for black hole formation falls when the Universe undergoes phase transitions, to produce a mass spectrum dominated by the horizon masses at the transition epochs (Jedamzik & Niemeyer 1999). Bullock & Primack (1997) argued that non-Gaussian density fluctuations produced during inflation could prevent over-production of

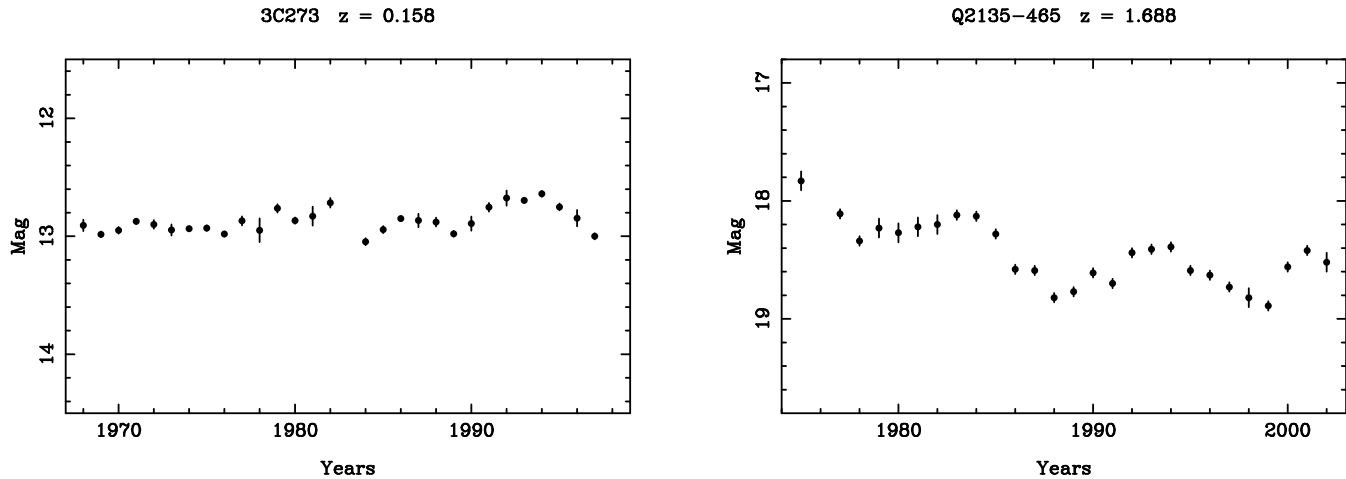


Figure 10. The left hand panel shows the V band light curve for the nearby quasar 3C273 from the 3C273 database at <http://isdc.unige.ch/3c273>. The right hand panel shows the B_J -band light curve for a high-redshift quasar from the Field 287 survey.

black holes, as well as providing a source of large amplitude fluctuations. This would be consistent with black hole production at the QCD mass scale, although Widerin & Schmid (1998) claimed that some additional fine tuning would be necessary. Yokoyama (1997) adopted a different approach, making the case that for inflation models with multiple scalar fields, isocurvature fluctuations are generated which, with a suitable choice of model parameters, produce primordial black holes with masses peaked at the MACHO mass scale. This idea has been developed (Kawaguchi et al. 2008; Frampton et al. 2010) in the context of the double inflation models. In this framework, primordial black holes with a narrow mass distribution can be produced in sufficient abundance to make up the dark matter, and with natural values for the model parameters will produce masses in the MACHO range.

7 DISCUSSION

For the last 20 years or so there has been a generally held view that dark matter is predominantly in the form of elementary particles. This is based in part upon the belief that there are no other suitable non-baryonic candidates, but it is also motivated by the limits on MACHOs derived from microlensing studies. This paper has set out to make the case that stellar mass primordial black holes provide viable alternative candidates. These bodies are not sufficiently massive to form luminous accretion discs, and can only be detected through the effects of gravitation, in particular gravitational lensing. In the case of bodies of around a solar mass, the changes in the lensing pattern have a timescale of the order of several years, which opens up the possibility of detecting them by observations of microlensing.

If primordial black holes make up a substantial proportion of dark matter, then every line of sight will be distorted at some level by gravitational lensing (Press & Gunn 1973). This means that for compact light sources such as quasars, the effects of microlensing should be detectable in their light

curves. Variations due to microlensing exhibit a number of well-defined characteristics which, if observed, would thus indicate the presence of primordial black holes. In Section 2 we focus on four properties of the light curves that should be present if the variations in flux are predominantly the result of microlensing. Ideally, one would like to compare the predictions for microlensing and for models of intrinsic variation such as accretion disc instability, with observed quasar light curves. Unfortunately, at present no models of intrinsic variation make predictions that are sufficiently precise to be useful for comparison with observations. Microlensing on the other hand results in specific predictions which can be tested experimentally.

There is one test which can distinguish between microlensing and intrinsic variations, in spite of the difficulties of modelling the latter. The absence of time dilation seen in Fig. 2 is not consistent with any mechanism for intrinsic variability in quasars, but it is in agreement with the predictions for microlensing. Of the other three properties of quasar light curves described in Section 2, none can strictly speaking exclude intrinsic variation, given the lack of constraint on models of quasar emission. However, the purpose of this paper is to show that the observations are consistent with the much more precise predictions for microlensing by primordial black holes. Microlensing simulations allow one to predict the shape of the light curve SEDs, and as can be seen from Fig. 1 there is good agreement with the observations. Without this agreement the case for microlensing would be severely weakened.

The question of colour changes with variation in flux is more complicated. It is well known that gravitational lensing is essentially an achromatic process (Schneider et al. 1992), with the expectation that for microlensing there will no change in colour with brightness. However, in the case of a resolved source, that is a source significantly larger than the Einstein radius of the lenses, this will not necessarily be true. For example, if the source has a radial colour gradient, blue in the centre and reddening outwards, then the

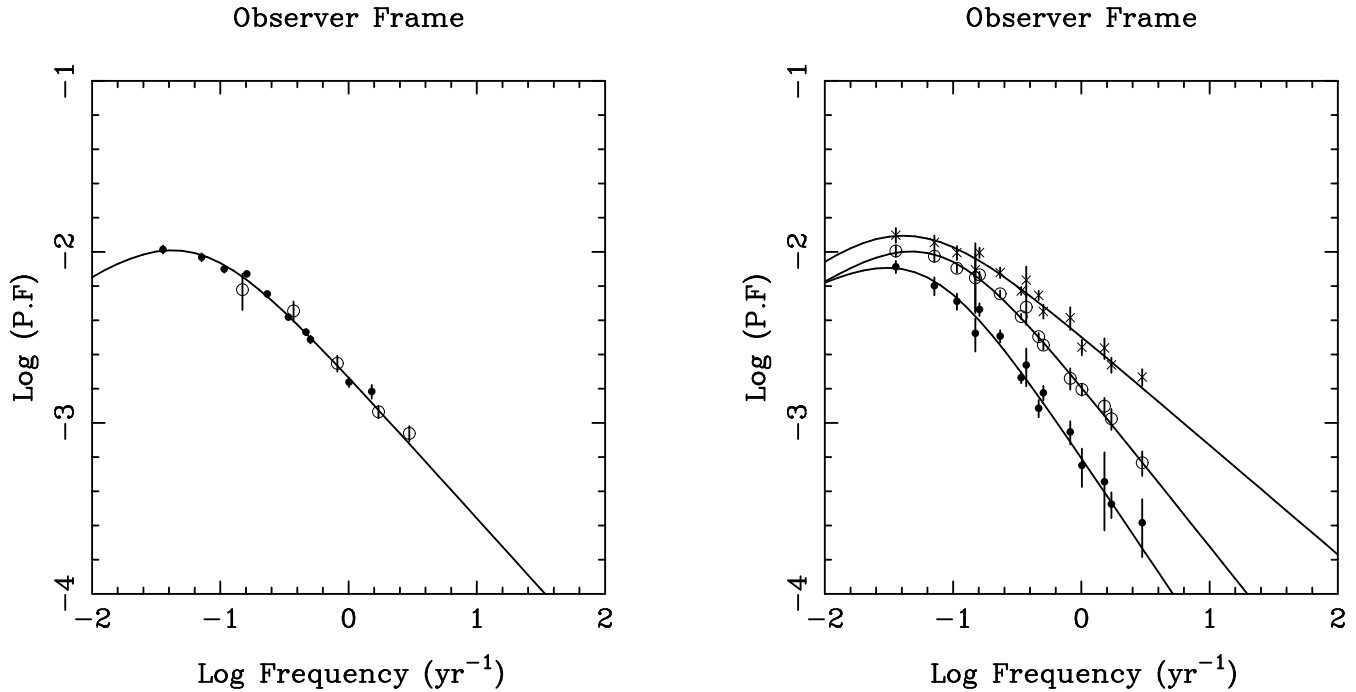


Figure 11. The left hand panel shows SEDs of light curves in the observer frame for quasars from the Field 287 survey (filled circles) and from the MACHO project (open circles). The solid line is the best fit of the curve in Eq. 7. The right hand panel shows the same data divided into three magnitude ranges. In this case filled circles, open circles and stars represent high, medium and low luminosity bins respectively. Solid lines are fits to the data as for the left hand panel

blue light profile, being more compact, will be preferentially amplified relative to the red as the lenses cross the source (Refsdal & Stabell 1991). In fact, as we have seen in Section 3, for bodies around a solar mass the Einstein radius is typically much larger than the quasar accretion disc and so the variations are expected to be achromatic. This is what was found for the quasar light curves analysed in Section 2, in agreement with the predictions for primordial black holes. Another property predicted for light curves from microlensing is statistical symmetry, and again the results in Section 2 show no evidence for asymmetry. It is not clear to what extent predictions for intrinsic variations favour symmetry. Despite the work of Kawaguchi et al. (1998), they are most likely to be model and timescale dependent. The point of significance for this paper is that all the features of quasar light curves analysed here are consistent with the predictions for microlensing by solar mass primordial black holes.

Changes in quasar spectra with variations in brightness provide an alternative way of testing for the presence of compact bodies. There is abundant evidence that broad emission lines respond to changes in continuum brightness, but the presence of a near critical density of primordial black holes implies that the continuum source will also vary with no corresponding change in broad line strength as a result of microlensing. This is clearly seen in Figs 6 and 7, and the evidence points to longer timescales of variation being associated with microlensing events. In the case of multiple quasar systems, the intrinsic features seen in both light curves, and used to measure time delay, are typically of small ampli-

tude and duration. On the other hand, microlensing events as measured from the difference between the light curves of individual images tend to be of large amplitude and to last for tens of years, as seen in Fig. 9.

The various constraints discussed above suggest a picture in which for low luminosity Seyfert I galaxies, observed variations are dominated by short timescale changes in flux accompanied by changes in colour and broad emission line strength. For more luminous quasars the amplitude of these intrinsic variations decreases, and at higher redshift the light curves become dominated by the effects of microlensing, as illustrated in Fig. 10. These variations occur on a longer timescale of around 20 years, are close to being achromatic, and do not affect the broad line region. The expectation from Eq. 9 is that with increasing luminosity, the amplitude of variation will become smaller as the size of the emitting region gets larger.

The idea that there is a correlation between the way quasars vary and their absolute magnitude or luminosity has a long history. In particular, several authors (Hook et al. 1994; Cristiani et al. 1996; Hawkins 2000) have claimed to find an anti-correlation between luminosity and amplitude, in the sense that for a sample of quasar light curves, more luminous quasars are seen to vary over a smaller range of brightness than less luminous ones. One of the problems with this conclusion is that the observed amplitude is clearly a function of the length of the run of observations, and so can be confused with timescale of variability. Fourier analysis provides a way round this by giving measures of variability on different timescales. The left

hand panel of Fig. 11 shows the combined SED for the samples of light curves described in Section 2, and fitted with the function $P(f)$ in Eq. 7. In the right hand panel the data is divided into three luminosity ranges, $M_B > -23.5$, $-25.5 < M_B < -23.5$ and $M_B < -25.5$. The three curves show broadly the same features as the curve in the left hand panel, but it is clear that the anti-correlation between luminosity and amplitude is confirmed. The maximum power density of the lowest luminosity quasars is greater than the highest by a factor of 1.5. In this case it appears that the time span of the data is sufficient to resolve the degeneracy between timescale and amplitude. This is consistent with the model outlined above.

For some time here has been a tendency to dismiss the idea that dark matter is in the form of primordial black holes or other compact bodies on the grounds that the MACHO collaboration observations of LMC stars have conflicted with predictions of the microlensing event rate. This would mean the falsification of the theory, regardless of the arguments in its favour (Popper 1959). We have shown in Section 4 that using more recent parameters for Galactic structure and dynamics there need be no discrepancy between predicted and observed event rates, and hence there are viable halo models where the dark matter is in the form of stellar mass compact bodies. The results of Section 5 even suggest that such bodies may have already been routinely detected in photometric monitoring of multiply lensed quasar systems. This means that the case for primordial black holes as dark matter can be considered on its merits, and contrasted with arguments favouring dark matter in the form of elementary particles.

8 CONCLUSIONS

The main conclusion of this paper is that stellar mass primordial black holes are plausible dark matter candidates. These objects would have been created during the QCD phase transition at a cosmic epoch of around 10^{-5} sec. Such bodies are not easy to detect, but should betray their presence through the effect of their gravitational fields. The most readily observable manifestation of this is the gravitational microlensing of quasars.

We have used power Fourier spectrum analysis of a large sample of quasar light curves to compare with the results of numerical simulations, and the predictions for time dilation, colour change and statistical symmetry from microlensing by a near critical density of primordial black holes. We have also compared the predictions for spectral changes as a result of microlensing with spectrophotometric observations of quasars. Finally, we make the case that the observed microlensing in multiple quasar systems is best explained by a population of dark matter bodies rather than stars.

The main objection to the idea of dark matter in the form of compact bodies has come from the search for MACHOs in the Galactic halo. By observing the microlensing rate of stars in the Magellanic Clouds, and adopting a dark matter model for the halo, the MACHO collaboration deduced a mass fraction in compact bodies of around 20%. We have re-worked their analysis using the most recent values for the structure and dynamics of the halo, and

find that there is now no conflict between the observed microlensing rate and a MACHO dominated halo.

The results of this paper do not establish that dark matter is made up of stellar mass primordial black holes. However, they do show that if it is in that form, then a wide variety expected signatures are confirmed by observation. On this basis, primordial black holes should be seen as viable alternatives to elementary particles in the search for the identification of dark matter.

ACKNOWLEDGEMENTS

This paper is based in part on SuperCOSMOS measurements of UK Schmidt Telescope plates. Data are available online through the SuperCOSMOS Science Archive: <http://surveys.roe.ac.uk/ssa>

REFERENCES

- Alcock C. et al., 1995, ApJ, 449, 28
- Alcock C. et al., 1996, ApJ, 461, 84
- Alcock C. et al., 1997, ApJ, 486, 697
- Alcock C. et al., 2000a, ApJ, 542, 281
- Alcock C. et al., 2000b, ApJS, 136, 439
- Alcock C. et al., 2001, ApJ, 550, L169
- Bennett D.P., Becker A.C., Tomaney A., 2005, ApJ, 631, 301
- Bernstein G., Fischer P., Tyson J.A., Rhee G., 1997, ApJ, 483, L79
- Bullock J.S., Primack J.R., 1997, Phys. Rev. D, 55, 7423
- Carr B.J., 1975, ApJ, 201, 1
- Carr B.J., 1994, ARA&A, 32, 531
- Carr B.J., Hawking S.W., 1974, MNRAS, 168, 399
- Chang K., Refsdal S., 1979, Nat, 282, 561
- Clavel J. et al., 1991, ApJ, 366, 64
- Cristiani S., Trentini S., La Franca F., Aretxaga I., Andreani P., Vio R., Gemmo A., 1996, A&A, 306, 395
- Donato F., Gentile G., Salucci P., 2004, MNRAS, 353, L17
- Evans N.W., 1994, MNRAS, 267, 333
- Feng J.L., 2010, ARA&A, 48, 495
- Frampton P.H., Kawasaki M., Takahashi F., Yanagida T.T., 2010, J. Cosmol. Astropart. Phys., 04, 023
- Geha M. et al., 2003, AJ, 125, 1
- Gilmore G., 1999, in Spooner N.J.C., Kudryavtsev V., eds, *The Identification of Dark Matter*. World Scientific, Singapore
- Griest K., 1991, ApJ, 366, 412
- Hawking S.W., 1971, MNRAS, 152, 75
- Hawkins E. et al., 2003, MNRAS, 346, 78
- Hawkins M.R.S., 1993, Nat, 366, 242
- Hawkins M.R.S., 1996, MNRAS, 278, 787
- Hawkins M.R.S., 2000, A&AS, 143, 465
- Hawkins M.R.S., 2003, MNRAS, 344, 492
- Hawkins M.R.S., 2007, A&A, 462, 581
- Hawkins M.R.S., 2010, MNRAS, 405, 1940
- Holmberg J., Flynn C., 2004, MNRAS, 352, 440
- Hook I.M., McMahon R.G., Boyle B.J., Irwin M.J., 1994, MNRAS, 268, 305
- Huchra J., Gorenstein M., Kent S., Shapiro I., Smith G., Horne E., Perley, R., 1985, AJ, 90, 691

- Hudson M.J., Smith R.J., Lucey J.R., Branchini E., 2004, MNRAS, 352, 61
- Irwin M.J., Webster R.L., Hewitt P.C., Corrigan R.T., Jedrzejewski R.I., 1989, AJ, 98, 1989
- Jedamzik K., 1997, Phys. Rev. D, 55, 5871
- Jedamzik K., Niemeyer J.C., 1999, Phys. Rev. D, 59, 124014
- Jurić M. et al., 2008, ApJ, 673, 864
- Kashlinsky A., Atrio-Barandela F., Kocevski D., Ebeling H., 2008, ApJ, 686, 49
- Kaspi S., Maoz D., Netzer H., Peterson B.M., Vestergaard M., Jannuzi B.T., 2005, ApJ, 629, 61
- Kaspi S., Brandt W.N., Maoz D., Netzer H., Schneider D.P., Shemmer O., 2007, ApJ, 659, 997
- Kawaguchi T., Mineshige S., Umemura M., Turner E.L., 1998, ApJ, 504, 671
- Kawaguchi T., Kawasaki M., Takayama T., Yamaguchi M., Yokoyama J., 2008, MNRAS, 388, 1426
- Kayser R., Refsdal S., Stabell R., 1986, A&A, 166, 36
- Kochanek C.S., 2004, ApJ, 605, 58
- Kogut A. et al., 1993, ApJ, 419, 1
- Korchagin V.I., Girard T.M., Borkova T.V., Dinescu D.I., van Altena W.F., 2003, AJ, 126, 2896
- Kuijken K., Gilmore G., 1991, ApJ, 367, L9
- Lewis G.F., Miralda-Escudé J., Richardson D.C., Wambsganss J., 1993, MNRAS, 261, 647
- McLaughlin D.E., van der Marel R.P., 2005, ApJS, 161, 304
- Minty E.M., 2001, PhD thesis, Univ. Edinburgh
- Minty E.M., Heavens A.F., Hawkins M.R.S., 2002, MNRAS, 330, 378
- Morgan C.W., Kochanek C.S., Morgan N.D., Falco E.E., 2010, ApJ, 712, 1129
- Ojha D.K., 2000, JApA, 21, 53
- Olling R.P., Merrifield M.R., 2000, MNRAS, 311, 361
- Paczynski B., 1986a, ApJ, 301, 503
- Paczynski B., 1986b, ApJ, 304, 1
- Pelt J., Schild R., Refsdal S., Stabell R., 1998, A&A, 336, 829
- Peterson B.M. et al., 2002, ApJ, 581, 197
- Popper K., 1959, *The Logic of Scientific Discovery*, Hutchinson: London
- Press W.H., Gunn J.E., 1973, ApJ, 185, 397
- Refsdal S., Stabell R., 1991, A&A, 250, 62
- Reid M.J., Readhead A.C.S., Vermeulen R.C., Treuhaft R.N., 1999, ApJ, 524, 816
- Schild R., Thomson D.J., 1995, AJ, 109, 1970
- Schneider P., Weiss A., 1987, A&A, 171, 49
- Schneider P., Ehlers J., Falco E.E., 1992, *Gravitational Lenses*, Springer: New York
- Siebert A., Bienaymé O., Soubiran C., 2003, A&A, 399, 531
- Siegel M.H., Majewski S.R., Reid I.N., Thompson I.B., 2002, ApJ, 578, 151
- Smith M.S., Kawano L.H., Malaney R.A., 1993, ApJS, 85, 219
- Timmer J., König M., 1995, A&A, 300, 707
- Turner E.L., Ostriker J.P., Gott J.R., 1984, ApJ, 284, 1
- Vietri M., Ostriker J.P., 1983, ApJ, 267, 488
- Walsh D., Carswell R.F., Weymann R.J., 1979, Nat, 279, 381
- Widerin P., Schmid C., 1998, unpublished (astro-ph/9808142)
- Wilhite B.C., Vanden Berk D.E., Brunner R.J., Brinkmann J.V., 2006, ApJ, 641, 78
- Xue X.X. et al., 2008, ApJ, 684, 1143
- Yokoyama J., 1997, A&A, 318, 673